INTERNATIONAL JOURNAL OF OPTIMIZATION IN CIVIL ENGINEERING
Int. J. Optim. Civil Eng., 2016; 6(4):523-547

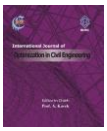

INVESTIGATION OF THE OPTIMAL SEMI-ACTIVE CONTROL STRATEGIES OF ADJACENT BUILDINGS CONNECTED WITH MAGNETORHEOLOGICAL DAMPERS

Mehmet E Uz[1] and P. Sharafi[2*, †]
[1]*Department of Civil Engineering, Adnan Menderes University, Aydin, PK:09100, Turkey*
[2]*Institute for Infrastructure Engineering, Western Sydney University, Penrith NSW 2751, Australia*

ABSTRACT

This study investigates the efficacy of optimal semi-active dampers for achieving the best results in seismic response mitigation of adjacent buildings connected to each other by magnetorheological (MR) dampers under earthquakes. One of the challenges in the application of this study is to develop an effective optimal control strategy that can fully utilize the capabilities of the MR dampers. Hence, a SIMULINK block in MATLAB program was developed to compute the desired control forces at each floor level and to the obtain number of dampers. Linear quadratic regulator (LQR) and linear quadratic Gaussian (LQG) controllers are used for obtaining the desired control forces, while the desired voltage is calculated based on clipped voltage law (CVL). The control objective is to minimize both the maximum displacement and acceleration responses of the structure. As a result, MR dampers can provide significant displacement response control that is possible with less voltage for the shorter building.

Keywords: seismic effects; adjacent buildings; semi-active control; clipped optimal algorithm; magneto-rheological (MR) damper.

Received: 26 January 2016; Accepted: 23 April 2016

1. INTRODUCTION

Various types of control devices have been widely utilized as supplemental damping strategies in order to mitigate the effects of earthquakes and high wind load on civil

[*]Corresponding author: Institute for Infrastructure Engineering, Western Sydney University, Penrith NSW 2751, Australia
[†]E-mail address: p.sharafi@westernsydney.edu.au (P. Sharafi)

engineering structures [1-7]. Dampers have been used onto structures as paramount interest over the past two decades. These dampers include fluid visco-elastic dampers [8-11], friction dampers [8-11], active devices [12-15] and semi-active magnetorheological (MR) dampers [16-19]. Westermo [20] was the first to propose the concept of linking the podium structure to the main buildings for avoiding the pounding effects. Westermo [20] found that this concept can be applied to mitigate the problem of pounding between the podium structure and the main building. Dyke et al. [21], Ni et al. [22] and Yoshida and Dyke [23] have investigated the effectiveness of magnetorheological (MR) dampers for civil engineering structures. Despite the recent development of control strategies like semi-active control, research in the area of passive and active structural control is still continuing [24].

Recent generation of the optimization approaches are being widely used for solving complex problems in structural engineering [25-30].Optimizing the use of dampers to mitigate seismic damage has hitherto not been investigated in spite of enhancing structural control concepts in the structural vibration control through the application of optimization. Luco and De Barros [31] investigated the optimal damping values for the distribution of passive dampers interconnecting two adjacent structures. In general, analytical and experimental studies have investigated the dynamic responses of the structures before and after installing a damping device to understand their effectiveness. However, very few studies have been undertaken with regard to the effect of non-uniform distribution of the dampers [10, 12, 32, 33]. None of these studies show a clear comparison in order to indicate the quality of their own proposed arrangement/solution. For example, Bhaskararao and Jangid [12] proposed a parametric study to investigate the optimum slip force of the dampers in the responses of two adjacent structures. The authors also showed that the response reduction is associated with optimum placement of damper.

Control algorithms developed for passive, semi-active and active control have been directly useful for developing other recent control strategies. The most common optimal control algorithms such as Linear Quadratic Regulator (LQR), H_2/LQG (Linear Quadratic Gaussian), H_2, H_∞ and fuzzy control can be chosen. Ahlawat and Ramaswamy [34] proposed an optimum design of dampers using a multi-objective version of the GA. Although a passive control technique is still considered due to its simplicity, semi-active and active control systems nowadays have received considerable attention. Arfiadi and Hadi [35] improved a simple optimization procedure with the help of genetic algorithms (GAs) to design the control force. They used a static output feedback controller utilizing the measurement output. In this case, the control force is obtained by multiplying the measurement with the gain matrix [35]. The performance of the controllers used in this study is also compared under two optimization controls. The aim is to obtain the optimum controller for MR dampers by using LQR and H_2/LQG strategies. The responses of the adjacent buildings are compared with the corresponding uncontrolled individual buildings. Numerical results of adjacent buildings controlled with MR dampers and the corresponding uncontrolled result are examined and compared with nonlinear control algorithms.

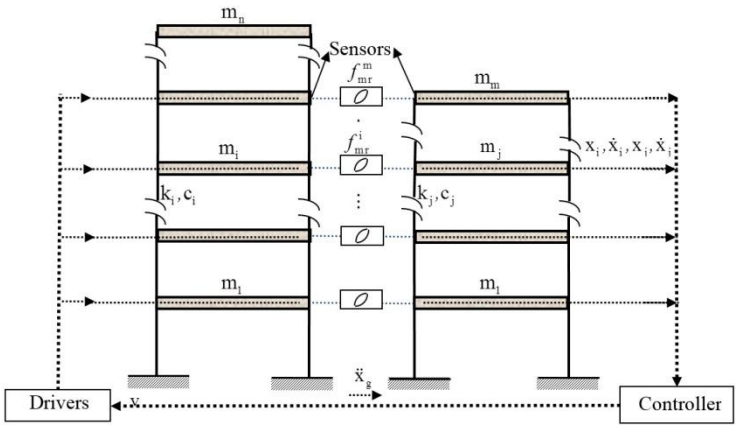

Figure 1. n and m storey shear buildings with MR dampers

2. THEORETICAL BACKGROUND OF SYSTEM MODEL

Consider two n and m storey shear buildings with semi-active dampers installed between them as shown in **Error! Reference source not found.**. Equations of motion of the adjacent buildings are shown in Eqs. (1) and (2). Equations of motion for the adjacent buildings having flexible columns and mass concentrated at the rigid slabs can be obtained by writing the equilibrium equations from the free body diagram of each of the lumped mass of the building.

Equation of motion of Building A:

$$M_1\ddot{X}_1 + C_1\dot{X}_1 + K_1X_1 = -M_1E_1\ddot{X}_g \tag{1}$$

Equation of motion of Building B:

$$M_2\ddot{X}_2 + C_2\dot{X}_2 + K_2X_2 = -M_2E_2\ddot{X}_g \tag{2}$$

Eqs. (1) and (2) should be solved simultaneously. When semi-active control is considered, a convenient matrix form can be developed by first combining these equations thus leading to the expression

$$\begin{bmatrix} M_1 & 0 \\ 0 & M_2 \end{bmatrix} \begin{Bmatrix} \ddot{X}_1 \\ \ddot{X}_2 \end{Bmatrix} + \left(\begin{bmatrix} C_1 & 0 \\ 0 & C_2 \end{bmatrix} + \begin{bmatrix} c_{d(m,m)} & 0_{(m,s)} & -c_{d(m,m)} \\ 0_{(s,m)} & 0_{(s,m)} & 0_{(s,m)} \\ -c_{d(m,m)} & 0_{(m,s)} & c_{d(m,m)} \end{bmatrix} \right) \begin{Bmatrix} \dot{X}_1 \\ \dot{X}_2 \end{Bmatrix}$$
$$+ \left(\begin{bmatrix} K_1 & 0 \\ 0 & K_2 \end{bmatrix} + \begin{bmatrix} k_{d(m,m)} & 0_{(m,s)} & -k_{d(m,m)} \\ 0_{(s,m)} & 0_{(s,m)} & 0_{(s,m)} \\ -k_{d(m,m)} & 0_{(m,s)} & k_{d(m,m)} \end{bmatrix} \right) \begin{Bmatrix} X_1 \\ X_2 \end{Bmatrix} = \begin{bmatrix} -M_1E_1 \\ -M_2E_2 \end{bmatrix} \ddot{X}_g + \begin{bmatrix} P_1 \\ P_2 \end{bmatrix} F_{mr}(t) \tag{3}$$

Equations of motion in Eq. (3) can be transformed into first order state equations. $c_{d(m,m)}$ and $k_{d(m,m)}$ are diagonal matrices of the additional damping and stiffness matrices due to the instillation of the MR dampers. The subscript of s in Eq. (3) denotes the $(n-m)$ difference of the number of storey levels of both buildings. By defining the state vector $X=\{X_1 \quad X_2 \quad \dot{X}_1 \quad \dot{X}_2\}^T$,

$$\Lambda=\begin{bmatrix} P_1 \\ 0 \\ P_2 \end{bmatrix}, \Gamma=\begin{bmatrix} -M_1E_1 \\ -M_2E_2 \end{bmatrix}, A=\begin{bmatrix} 0_{(n+m)\times(n+m)} & \mathbf{I}_{(n+m)\times(n+m)} \\ -M^{-1}K & -M^{-1}C \end{bmatrix}$$
$$E=\begin{bmatrix} 0_{(n+m)\times 1} \\ M^{-1}\Gamma \end{bmatrix}, B=\begin{bmatrix} 0_{(n+m)\times n_a} \\ M^{-1}\Lambda \end{bmatrix} \tag{4}$$

where E_1 and E_2 are $n\times 1$ and $m\times 1$ unity matrices, respectively. P_1 and P_2 are dimensional matrices based on the number of actuators of the additional dampers. m denotes the storey number of the lower building. Here, **I** is an identity matrix and 0 in matrix Λ is a $(s\times n_a)$ matrix containing zero. $F_{mr}=\begin{bmatrix} f_{mr}^1 & \cdots & f_{mr}^i & f_{mr}^m \end{bmatrix}^T$ is control input vector.

$$\begin{aligned} \dot{X} &= AX+BF_{mr}(t)+E\ddot{X}_g(t) \\ x &= C_wX+D_wF_{mr} \\ y_m &= C_mX+D_mF_{mr}+v \end{aligned} \tag{5}$$

In which y_m is the vector of measured outputs, x is the regulated output vector and v is the measurement noise vector. Since only earthquake loading is considered without MR dampers, the equations of motion can be written as

$$\dot{X}=AX+E\ddot{X}_g(t) \tag{6}$$

Eq. (6) defines the uncontrolled adjacent buildings system in order to understand the efficiency of MR dampers between both buildings.

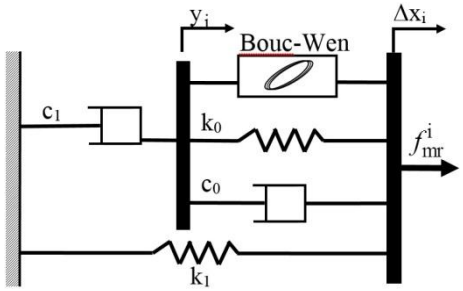

Figure 2. Modified Bouc- Wen model for MR damper [36]

3. DYNAMIC MODEL OF MR DAMPER FORCES

The modified Bouc-Wen model as shown in **Error! Reference source not found.** is used to simulate the dynamic behaviour of the MR damper as [36]

$$f_{mr}^{i} = c_1\dot{y}_i + k_1\left(x_{i+n} - x_i - x_0\right) \tag{7}$$

where the internal pseudo-displacement, $\dot{y}_i$ and the evolutionary variable, $\dot{z}_{di}$ are given by

$$\begin{aligned}\dot{y}_i &= \frac{1}{\left(c_0 + c_1\right)}\left\{\alpha z_{di} + c_0\left(\dot{x}_{n+i} - \dot{x}_i\right) + k_0\left(x_{n+i} - x_i - y_i\right)\right\} \\ \dot{z}_{di} &= -\gamma\left|\dot{x}_{n+i} - \dot{x}_i - \dot{y}_i\right|z_{di}\left|z_{di}\right|^{n_d-1} - \beta\left(\dot{x}_{n+i} - \dot{x}_i - \dot{y}_i\right)\left|z_{di}\right|^{n_d} + A_c\left(\dot{x}_{n+i} - \dot{x}_i - \dot{y}_i\right)\end{aligned} \tag{8}$$

where x_{n+i} and x_i are the displacements of the i^{th} floor of Building B and Building A, respectively. The displacement of the MR damper Δx_i is computed using the relative displacement between two inline adjacent floors (i). x_0 is the initial displacement of spring of the accumulator stiffness $k_1 . k_0$ is the stiffness at large velocities. c_0 and c_1 are viscous damping coefficients at large velocities and for force roll-off at low velocities, respectively. α is the evolutionary coefficient. Other shape parameters of the hysteresis loop are shown as γ, A_c, n_d and β in Eq. (8). In this model, the following three model parameters depend on the command voltage *u* to the current driver are expressed as follows:

$$\alpha = \alpha_a + \alpha_b u_i\,;\; c_1 = c_{1a} + c_{1b}u_i\,;\; c_0 = c_{0a} + c_{0b}u_i \tag{9}$$

Eq. (10) simulates the dynamics involved in both reaching rheological equilibrium and driving the electromagnet in the MR damper. The dynamics are accounted for through the first order filter

$$\dot{u} = -\eta\left(u_i - v_i\right) \tag{10}$$

where u_i is given as the output of a first-order filter which models delay dynamics of the current driver and of the fluid to reach rheological equilibrium. v_i is a command input voltage supplied to the damper at the i^{th} floor. f_{mr}^{i} is the damper force at the i^{th} floor level between the buildings. Parameters of the MR dampers used in this study were obtained by Spencer et al. [36] and are shown in **Error! Reference source not found.**.

Table 1: Parameters of Bouc-Wen phenomenological model parameters for 1000 kN MR dampers [33, 36]

Parameter	Value	Parameter	Value
C_{0a}	50.30 kN sec/m	α_a	8.70 kN/m
C_{0b}	48.70 kN sec/m/V	α_b	6.40 kN/m/V
k_0	0.0054 kN/m	γ	496.0 m^{-2}
C_{1a}	8106.2 kN sec/m	β	496.0 m^{-2}
C_{1b}	7807.9 kN sec/m/V	A_c	810.50
k_1	0.0087 kN/m	n_d	2
X_0	0.18 m	η	195 sec^{-1}

4. OPTIMAL CONTROLLER DESIGN

For the optimization of semi-active control problems between adjacent buildings, several optimization methods based on the chosen objective function have been synthesized in this study. H_∞ and LQR norms are used to obtain the optimum damper parameters.

4.1 H_∞ Optimization

To quantify the transfer functions H_∞ norm is usually used. In H_∞ controllers, the objective is to minimize the infinity norm of the transfer function from external disturbances to the regulated outputs. The H_∞ norm can be performed into the iterative manner [35]. In this case, Hamiltonian matrix can be defined as

$$\boldsymbol{H} = \begin{bmatrix} \mathrm{A} + \mathrm{E}R^{-1}\mathrm{D}^{\mathrm{T}}\mathrm{C}_{\mathrm{w}} & \mathrm{E}R^{-1}\mathrm{E}^{\mathrm{T}} \\ -\mathrm{C}_{\mathrm{w}}^{\mathrm{T}}\left(\mathrm{I} + \mathrm{D}R^{-1}\mathrm{D}^{\mathrm{T}}\right)\mathrm{C}_{\mathrm{w}} & -\left(\mathrm{A} + \mathrm{E}R^{-1}\mathrm{D}^{\mathrm{T}}\mathrm{C}_{\mathrm{w}}\right)^{\mathrm{T}} \end{bmatrix} \tag{11}$$

where $R = \gamma^2\mathrm{I} - \mathrm{D}^{\mathrm{T}}\mathrm{D}$. In this study, eigenvalues of this matrix in Eq. (11) are symmetric about the real and imaginary axes with D=0. The H_∞ norm can be computed in the following bisection algorithm

Select γ_u, γ_l so that $\gamma_l \le \left\|\hat{\mathrm{G}}_\infty\right\| \le \gamma_u$

If $\left(\gamma_u - \gamma_l\right)/\gamma_l \le$ specified level (Tol.)

Yes Stop ($\left\|\hat{\mathrm{G}}_\infty\right\| \approx \frac{1}{2}\left(\gamma_u + \gamma_l\right)$)

Otherwise go to Step (3)

Set $\gamma = \left(\gamma_u + \gamma_l\right)/2$ and test if $\left\|\hat{\mathrm{G}}_\infty\right\| \le \gamma$ using $\lambda_i\left(\boldsymbol{H}\right)$

If $\lambda_i\left(\boldsymbol{H}\right)$ j$\mathbb{R}$, then set $\gamma_l = \gamma$, otherwise set $\gamma_u = \gamma$ and go to Step (2)

The resulting γ is the H_∞ norm to be determined. In the numerical solution, the computation of H_∞ norm in bisection algorithm can be obtained by using *norm* commands in

the MATLAB Control System Toolbox [37]. The damper parameters were then solved using genetic based optimizer. Note that the displacements and velocities of the adjacent buildings can be included to the controlled output defined in Eq. (5). By choosing the appropriate entry in the regulation matrix, certain regulated output that needs to be minimized can be imposed. For example, if the regulated output is taken as the relative displacement and velocities of the floors of both buildings with respect to the ground, matrix C_w can be chosen as

$$\begin{aligned} C_w &= C_m = [\boldsymbol{I}] \\ D_w &= D_m = [\mathbf{0}] \end{aligned} \tag{12}$$

where $\boldsymbol{I}$ is a $(2n+2m)\times(2n+2m)$ identity matrix, 0 and $\mathbf{0}$ denote as $(2n+2m)\times 1$ vector and $(2n+2m)\times(m)$ matrix containing zeros, respectively. n and m are total degrees of freedom of both Building A and Building B. The optimization problem is to find the optimum damper parameters that minimize H_∞ in GA is used in the optimization tool.

4.2 LQR Optimization

The clipped-optimal control method is to solve an optimal control problem and to calculate the optimum force. For this purpose, LQR and H_2/LQG strategies are common in optimal control problems. Firstly, a LQR algorithm with full state feedback is employed in this study. For designing a LQR controller, the aim is to minimize the quadratic performance index $\mathbf{J} = \frac{1}{2}\int_0^\infty [x^T \mathbf{Q} x + F_{mr}^T \mathbf{R} F_{mr}]dt$ subject to state Eq. (5) without external excitation taken as the constraint [38]. Here, both $\mathbf{Q}$ positive semi-definite state and $\mathbf{R}$ the positive control input weighting matrices are for the vector of regulated responses, x in Eq. (5) and of control forces, F_{mr} respectively. Optimal control force vector can be written as [39, 40]

$$f_d = -B^T \mathbf{R}^{-1} P X = -\mathbf{K} X \tag{13}$$

where P is the solution of the algebraic Riccati equation as shown in Eq. (14).

$$PA + A^T P + C_w^T \mathbf{Q} C_w - PB\mathbf{R}^{-1}B^T P = 0 \tag{14}$$

For multiple MR dampers being considered, the control input is a vector, i.e. $f_d = [f_{d1} \quad \cdots \quad f_{di} \quad f_{dm}]^T$ and $\mathbf{R} = [R]$. $\mathbf{K}$ is the full state feedback gain matrix for the deterministic regulator problem. However, the number of sensors should be limited for economical reasons, the need of the output feedback, where not all states are available, is more pronounced [41].

4.3 LQG optimization

Many states in realistic systems are not easily measurable. The optimal controller in Eq. (13) is not implemental without the full state measurement [38, 42]. Hence, in this study a H_2/LQG controller is also employed as a nominal controller and the results are compared with the corresponding LQR controller. A state estimate can be formulated as $\hat{\mathrm{X}}$ that $\mathrm{f_d} = -\mathbf{K}\hat{\mathrm{X}}$ remains optimal based on the measurements [38]. Further, in the design of the H_2/LQG controller, the ground acceleration input, $\ddot{\mathrm{x}}_\mathrm{g}$ is taken to be a stationary white noise. An infinite horizon performance index is chosen as $\mathbf{J} = \lim_{\tau\to\infty}\frac{1}{\tau}\mathrm{E}\left[\int_0^\tau\left[\mathrm{y_m^T}\mathbf{Q}\mathrm{y_m} + \mathrm{F_{mr}^T}\mathbf{R}\mathrm{F_{mr}}\right]\mathrm{dt}\right]$. Both $\mathbf{Q}$ and $\mathbf{R}$ weighting matrices are for the vector of measured responses, $\mathrm{y_m}$ in Eq. (5) and of control forces, $\mathrm{F_{mr}}$ respectively.

$$\begin{aligned}\mathbf{Q} &= \mathrm{diag}\left[\mathrm{K} \quad \mathrm{M}\right]\\ \mathbf{R} &= \mathrm{r}\Lambda^\mathrm{T}\mathrm{K}\Lambda\end{aligned} \tag{15}$$

For design purposes, the measurement noise is assumed to be identically distributed, statistically independent Gaussian white noise processes with $\mathrm{S}_{\ddot{\mathrm{x}}_\mathrm{g}\ddot{\mathrm{x}}_\mathrm{g}}/\mathrm{S}_{v_\mathrm{i}v_\mathrm{i}} = \gamma_\mathrm{g} = 50$, where $\mathrm{S}_{\ddot{\mathrm{x}}_\mathrm{g}\ddot{\mathrm{x}}_\mathrm{g}}$ are $\mathrm{S}_{v_\mathrm{i}v_\mathrm{i}}$ the auto spectral density function of ground acceleration and measurement noise. The nominal controller is represented as [43]

$$\begin{aligned}\dot{\hat{\mathrm{X}}} &= \left(\mathrm{A} - \mathrm{L_g}\mathrm{C_m}\right)\hat{\mathrm{X}} + \mathrm{L_g}\mathrm{y_m} + \left(\mathrm{B} - \mathrm{L_g}\mathrm{D_m}\right)\mathrm{F_{mr}}\\ \mathrm{L_g} &= \left(\mathrm{C_m}\mathrm{S}\right)^\mathrm{T}\end{aligned} \tag{16}$$

where S is the solution of the algebraic Ricatti equation given in Eq. (18). $\hat{\mathrm{X}}$ is the optimal estimate of the state space vector, X. $\mathrm{L_g}$ is the gain matrix for state estimator with the state observer technique, which is determined by solving an algebraic Riccati equation in the control toolbox in MATLAB [37].

$$0 = \mathrm{S}\mathrm{A}^\mathrm{T} + \mathrm{A}\mathrm{S} - \mathrm{S}\mathrm{C_m^T}\mathrm{C_m}\mathrm{S} + \gamma_\mathrm{g}\mathrm{E}\mathrm{E}^\mathrm{T} \tag{17}$$

Based on selected displacement and velocity measurements, a Kalman filter is used to estimate the states. In order to produce an approximately desired control force, $\mathrm{f_d}$ a force feedback loop is appended for inducing the MR device. A linear optimal controller $K_\mathrm{c}(s)$ is designed that provides the desired control force, $\mathrm{f_d}$ based on the measured responses, $\mathrm{y_m}$ and the measured force, $\mathrm{F_{mr}}$ as follows

$$\mathrm{f_d} = L^{-1}\left\{-K_\mathrm{c}(s)\,L\left(\begin{bmatrix}\mathrm{y_m}\\ \mathrm{F_{mr}}\end{bmatrix}\right)\right\} \tag{18}$$

where $L(.)$ is the Laplace transform. Although the controller $K_\mathrm{c}(s)$ can be obtained from a variety of synthesis methods, the H_2/LQG strategies are conducted herein due to the stochastic nature of earthquake ground motions and because of their successful application in other civil engineering control applications [22, 42, 44]. Note that the damper is driven by the applied command input voltage, v. The states i.e. $(\mathrm{x},\mathrm{y},\mathrm{z_d},u)$ are obtained via integration of Eqs. (5), (8) and (10) using MATLAB module ode45 based on the $4^{\mathrm{th}}/5^{\mathrm{th}}$ - order Runge-Kutta method. Then, available damper force, $\mathrm{F_{mr}} = \begin{bmatrix} f_{\mathrm{mr}}^{1} & \cdots & f_{\mathrm{mr}}^{\mathrm{i}} & f_{\mathrm{mr}}^{\mathrm{m}} \end{bmatrix}^{\mathrm{T}}$ and the desired force $\mathrm{f_d}$ are obtained via Eqs. (7) and (13), respectively.

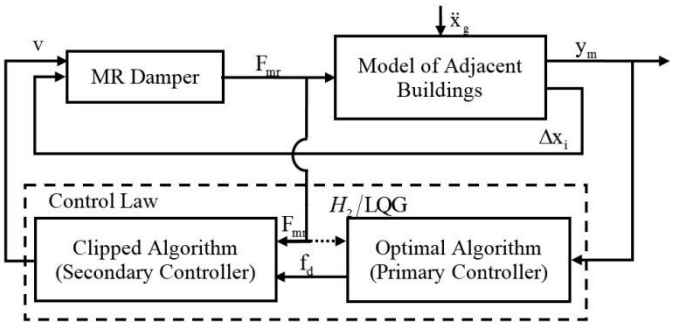

Figure 3. Semi-active control block diagram of LQR–CVL and $H_2/\mathrm{LQG}-\mathrm{CVL}$

4.4 CVL control

The schematic for implementations of LQR–CVL and $\mathrm{LQG}-\mathrm{CVL}$ are illustrated in **Error! Reference source not found.**. Inverting the damper dynamics to obtain command voltage for a desired force is not possible from Eqs. (8), (9) and (10). The first method is based on LQR–CVL and the second method is based on $H_2/\mathrm{LQG}-\mathrm{CVL}$. Hence, two methods are used to obtain the voltage, v as described below. Nonlinear force of damper is not directly controllable and applied voltage to the current driver can only be adjusted to reach the desired control force at each time step. The applied voltage is set after computation of the optimal control force by a predefined control algorithm according to feedback data and measurement of the damper force at each time in order to approach the MR damper control force to the desired optimal force. The input voltage, v, to the damper is obtained using the CVL [22] as described below. If these two forces are equal then the applied voltage is not changed. If the absolute of MR damper force is less than the absolute of the calculated optimal control force and both of them have the same sign, the applied voltage should be increased to its maximum value. Otherwise, the input voltage is set to zero. Clipped-optimal method can be summarized in the following equation.

$$v = V_{max}\mathbf{H}\left\{\left(f_d - F_{mr}\right)F_{mr}\right\} \tag{19}$$

where V_{max} shows the maximum applied voltage that is associated with saturation of magnetic field in MR damper and $\mathbf{H}\{.\}$ is the Heaviside function. The voltage applied to the MR damper should be V_{max} when $\mathbf{H}\{.\}$ is greater than zero. Otherwise, the command voltage is set to zero. **Error! Reference source not found.** shows a block diagram of the clipped optimal semi-active control system. The feedback for the controller is based on displacement measurements.

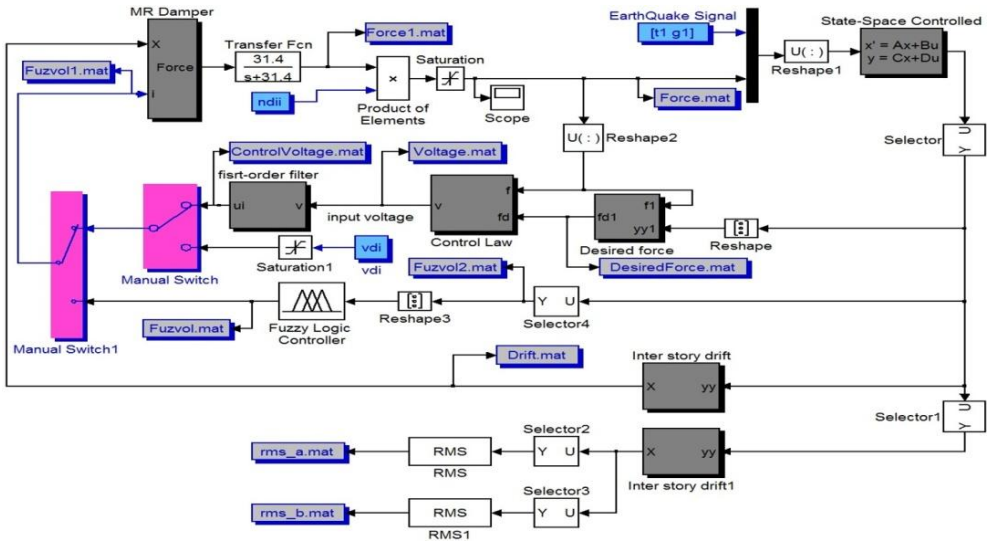

Figure 4. Block diagram of semi-active control system using H_2/LQG controller

5. SOLUTION PROCEDURE

A numerical example for adjacent buildings is performed on i7-2630QM @2.9 GHz computer running MATLAB R2011b. The MATLAB numeric computing environment is integrated into the SIMULINK block to simulate either LQR or H_2/LQG controller.

6. NUMERICAL STUDY

A system of buildings located adjacent to each other and interconnected by MR dampers is considered to obtain the optimal semi-active control strategies. Building A is a 20-storey shear building discussed in Bharti et al. [33] and Ok et al. [32]. A 10-storey building discussed in Pourzeynali et al. [45] is taken as Building B. The adjacent buildings are subjected to four earthquake ground motions El-Centro 1940, Kobe 1995 scaled to 0.8 g and 0.3 g, Sakarya 1999 and Loma Prieta 1989. The structural parameters having mass, stiffness

and damping coefficient are shown for both buildings in **Error! Reference source not found.**.

Table 2: The structural parameters of both buildings in numerical examples

Floor (i)	Building A			Building B		
	m_i (t)	$K_i \times 10^6$ (kN/m)	$c_i \times 10^3$ (kN sec/m)	m_i (t)	$K_i \times 10^5$ (kN/m)	$c_i \times 10^3$ (kN sec/m)
1	800	1.4	4.375	215	4.68	1.676
2	800	1.4	4.375	201	4.76	1.648
3	800	1.4	4.375	201	4.68	1.585
4	800	1.4	4.375	200	4.5	1.585
5	800	1.4	4.375	201	4.5	1.539
6	800	1.4	4.375	201	4.5	1.539
7	800	1.4	4.375	201	4.5	1.539
8	800	1.4	4.375	203	4.37	1.539
9	800	1.4	4.375	203	4.37	1.099
10	800	1.4	4.375	176	3.12	1.146
11	800	1.4	4.375			
12	800	1.4	4.375			
13	800	1.4	4.375			
14	800	1.4	4.375			
15	800	1.4	4.375			
16	800	1.4	4.375			
17	800	1.4	4.375			
18	800	1.4	4.375			
19	800	1.4	4.375			
20	800	1.4	4.375			

7. RESULTS OF ADJACENT BUILDINGS CONNECTED WITH MR DAMPERS

The peak top floor displacement, the peak top floor acceleration, the peak storey shear and the peak base shear are obtained with passive-off and passive-on cases which are with constant zero voltage and with constant maximum applied voltage (i.e., 3, 6 and 9 V), respectively and compared with semi active control cases based on LQR and LQG. **Error! Reference source not found.** shows the time response histories of top floor displacement of both buildings based on the considered four control strategies under the four different earthquakes and compared to uncontrolled case. In time variation responses, the Kobe 1995 earthquake scaled to 0.3 g is used in order to compare explicitly with other earthquakes considered in this study. As shown in **Error! Reference source not found.** (a), passive-on and semi-active based on both the LQR and LQG norms result in good agreement compared to passive-off under El-Centro 1940 and Sakarya 1999 earthquakes while all control strategies have the same trend in Kobe 1995 and Loma Prieta 1989 ground motions.

It is observed from **Error! Reference source not found.** (b), that all control strategies reduce the top floor displacement of Building B under all the considered earthquakes. In

terms of reduction of displacement responses, the performance of the control strategies in the lower building (Building B) is better than the higher building (Building A). **Error! Reference source not found.** indicates the time response histories of the top floor acceleration of Building A and Building B. The results in **Error! Reference source not found.** (a) indicate that for all control strategies the overall trend is similar to the uncontrolled case in Building A. **Error! Reference source not found.** (b) shows that semiactive controller based on LQG norm is effective in response mitigations for the lower building. The acceleration response reduction of Building B is higher under semiactive compared to passive-on strategy, except that under the 1999 Sakarya earthquake semiactive has the same trends with passive-off and on strategies. Although the response history of the top floor acceleration in the higher building is similar in passive-off and passive-on strategies, a comparative performance of the four strategies in Building B can be slightly observed in terms of acceleration responses.

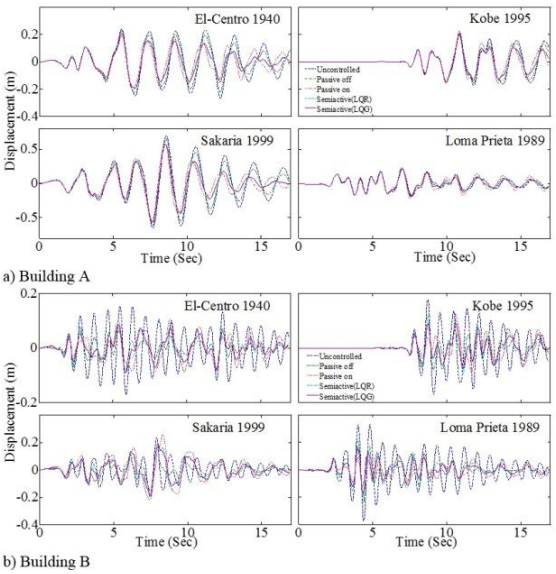

Figure 5. Time response of top floor displacement of a) Building A b) Building B

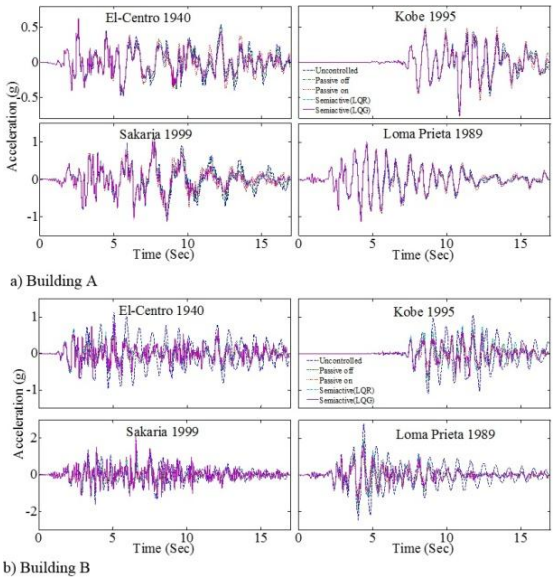

Figure 6. Time response of top floor acceleration a) Building A b) Building B

The response histories of the normalized base shear of both buildings are investigated in **Error! Reference source not found.**. The base shear of each building is normalized with the corresponding building weight. Therefore, the normalized base shear response of Building A is explicitly smaller than the normalized base shear response of Building B. Further, **Error! Reference source not found.** (a) indicates that semiactive controllers are in good agreement in the mitigation of the base shear. All controllers are showing better performance compared to the uncontrolled case in Kobe 1995 and El-Centro 1940 earthquakes. Although the MR dampers work as passive devices with the maximum damper command voltage (6V) under passive-on strategy, the response histories in terms of the normalized base shear in **Error! Reference source not found.** (a) are almost matching with the uncontrolled case. It is observed from **Error! Reference source not found.** (b), increase in base shear response is noted for Building B under passive-on strategy for Sakarya 1999 earthquake while all control strategies exhibit better control performance for the other three earthquakes.

After the comparative time history response plots, another comparative performance of the four control strategies is conducted in terms of the peak floor displacement acceleration and storey shear force based on the storey levels of both buildings. **Error! Reference source not found.** shows the peak floor displacement of Building A and Building B. It is noted from **Error! Reference source not found.** (a), that the control performance of both passive-on and semiactive controllers is better than passive-off. Under passive-on strategy, peak floor displacements of Building A in Kobe 1995 earthquake are not good in terms of displacement reduction. The results of semiactive control strategies in **Error! Reference source not found.** (a) and **Error! Reference source not found.** (b) are almost matching for both buildings. Similarly, the overall trend in terms of semiactive controllers is similar for the shorter building in **Error! Reference source not found.** (b). Under Sakarya 1999 and El-Centro 1940 earthquakes, passive-off strategy provides the best reduction compared to semiactive controllers. The displacement response mitigation for the higher floors of Building B is higher under semiactive compared to passive control strategies and the

uncontrolled case.

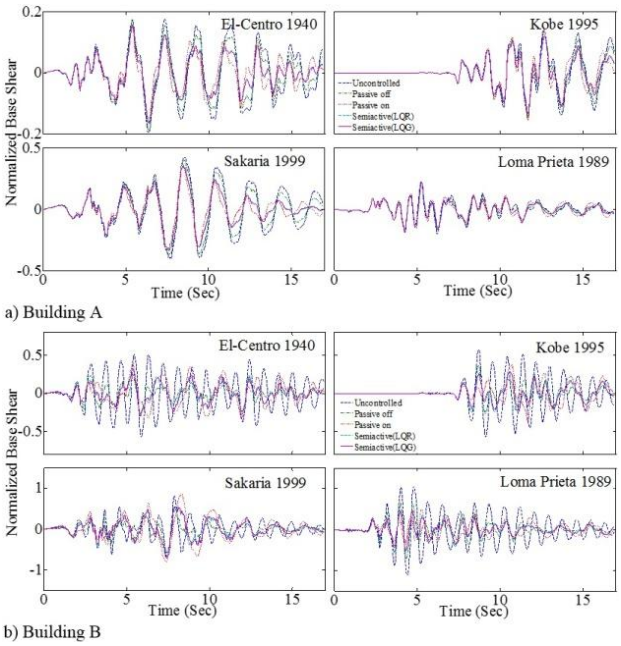

Figure 7. Time response history of base shear of a) Building A b) Building B

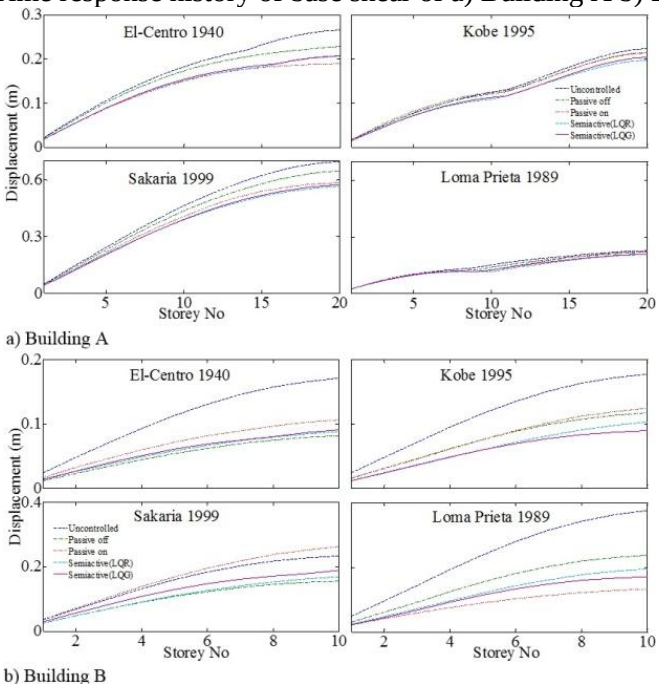

Figure 8. Peak floor displacement of a) Building A b) Building B

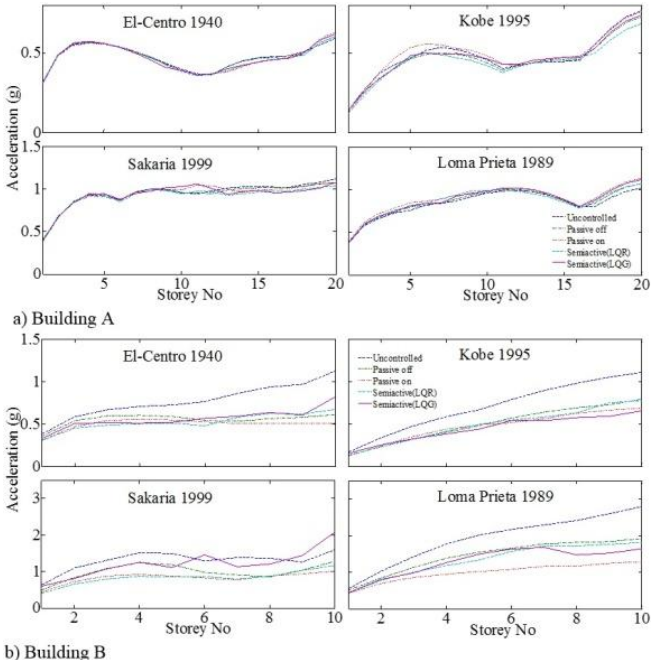

Figure 9. Peak floor acceleration of a) Building A b) Building B

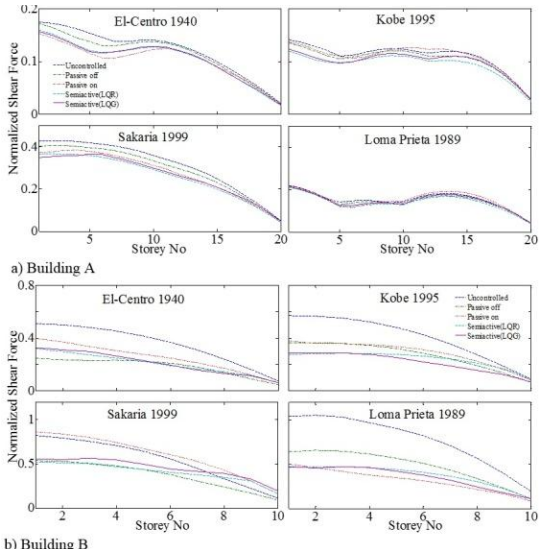

Figure 10. Peak storey shear of a) Building A b) Building B

Error! Reference source not found. shows the peak floor acceleration based on storey levels. It is observed from **Error! Reference source not found.** (a), that the control strategies are not showing better results compared to the uncontrolled case based acceleration reduction for the higher building (Building A). Increase in acceleration response is noted for higher floors under all control strategies for Kobe 1995 earthquake. On the other hand, all control strategies in acceleration response reduction for Building B are effective as depicted through **Error! Reference source not found.** (b). Semiactive controller based on LQR is showing

better mitigation than semiactive based on H_2/LQG for Building B. The acceleration reduction of the shorter building (Building B) is higher than the taller building (Building A). Further, it is interesting that passive-on strategy in **Error! Reference source not found.** (b) is showing better response in terms of mitigation of the peak floor acceleration than semiactive and passive-off strategies.

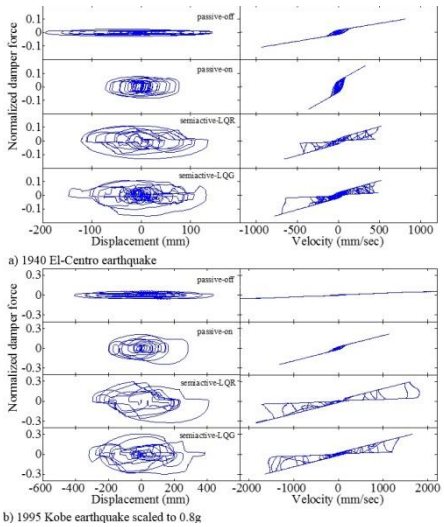

Figure 11. The Behaviour of MR damper under a) 1940 El-Centro earthquake b) 1995 Kobe earthquake scaled to 0.8g

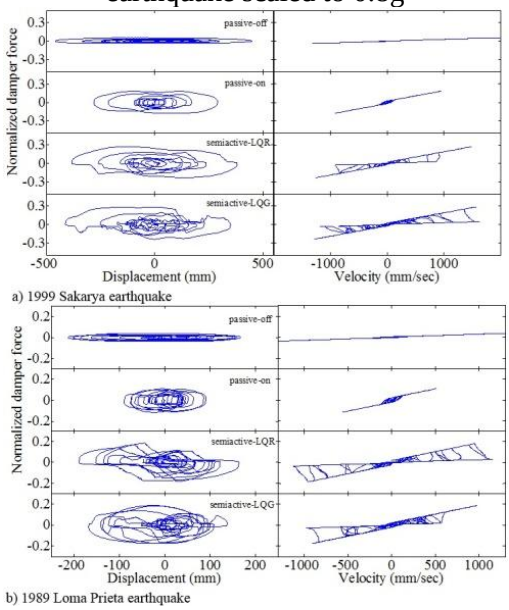

Figure 12. The Behaviour of MR damper under a) 1999 Sakarya earthquake b) 1989 Loma Prieta earthquake

Error! Reference source not found. shows the performance of the four control strategies in terms of storey shear for Building A and Building B. The overall best control

performance is observed under semiactive controllers for all considered ground motion, especially in Sakarya 1999 for Building A and in Kobe 1995 for Building B. Passive-on strategy for Building A in Kobe 1995 and Building B in Sakarya 1999 is not effective to reduce the storey shear. For Building A, Kobe 1995 and Loma Prieta 1989 earthquakes show increase in storey shear with increasing storey levels. This is due to the fact that the sway of Building A is abruptly restricted by Building B as it suffers high storey shear above the tenth floor. Hence, this limitation results in an increase in displacement response of Building A under passive-on strategy in Kobe 1995 and Loma Prieta 1989 earthquakes as depicted in **Error! Reference source not found.** (a). In **Error! Reference source not found.** (b) reduction in response for Building B is observed under all considered earthquakes, except to Sakarya 1999 ground motion. Passive-on and semiactive controllers showed a better control of response as shown in **Error! Reference source not found.** (b). Hysteresis behaviour of MR damper placed at the 10^{th} storey level between the buildings under four control strategies, namely, passive-off, passive-on, semiactive-LQR and semiactive-H_2/LQG for the four different earthquakes is shown in **Error! Reference source not found.** and **Error! Reference source not found.**. It is observed that there is a significant energy dissipation in terms of displacement and velocity responses of MR damper in semi-active based on LQR and LQG norms compared to passive-on $(V_{max} = 6V)$ and passive-off strategies. This study also investigated the influence of damper location and command voltage required for MR damper. In order to show the effectiveness of MR dampers for inter-connecting the 10th floors of two buildings having different characteristics, the numerical model is used for the two damper locations and for three values of command voltage (3V, 6V and 9V).

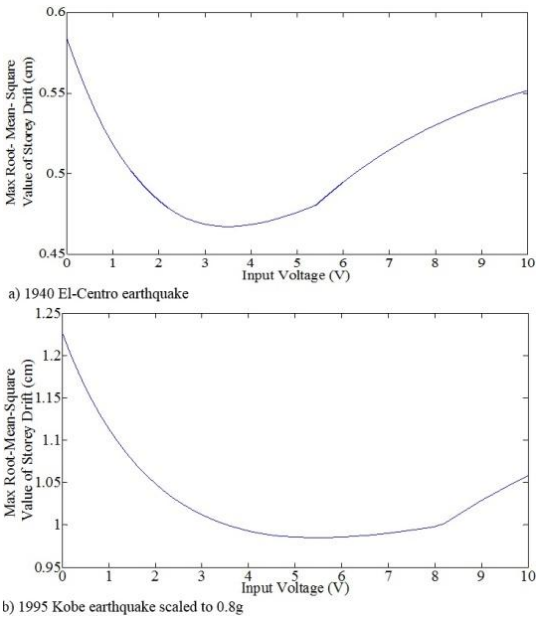

Figure 13. Control performance of MR dampers with uniform input voltages under the 1995 Kobe earthquake scaled to 0.8g (Uz and Hadi 2013)

The command voltages of MR dampers at each of the ten floors between the buildings are determined by the two proposed methods (LQR and LQG optimizations). Optimal input voltage distribution of fixed number of dampers is provided in this numerical example and compared to other control strategies. Five MR dampers installed at each of the ten floors in the numerical example. All 50 dampers have the same input voltage. Nonlinear random vibration analyses using the 4th order Runge Kutta method is performed while varying the uniform input voltage from 0 to 10 V, which leads to the variation of the damping capacity of the MR dampers. **Error! Reference source not found.** shows the maximum root-mean-square (r.m.s.) values of inter-storey drifts of the coupled systems by varying the uniform input voltage of MR damper under El-Centro 1940 and Kobe 1995 earthquakes. For decreasing the maximum inter-storey drift of the adjacent system, it is explained that an optimal value for the uniform input voltage of the MR dampers exists in a coupled structure system. In this numerical example, the optimal input voltage of the MR dampers is 5.6 V for the uniform distribution of the 50-MR damper system in Kobe 1995 earthquake, while the optimal input voltage is 3.1 V in El-Centro 1940 earthquake. Using the MR damper is important in damping capacity that can be easily adjusted by modulating the input voltage, without costly replacements or adjustments. In other words, varying the input voltages of the dampers is feasible in order to achieve an optimal performance. Hence, the results of the peak top floor displacement, acceleration and normalized base shear of the adjacent buildings using the optimum uniform voltage (OUV) is evaluated with the other control strategies used in this study. It is observed from **Error! Reference source not found.** that the overall displacement response reduction with passive-on strategy is as much with semiactive controllers except for passive-off for Building B in El-Centro 1940 earthquake.

Table 3: Peak top floor displacement under different control strategies

Earthquakes	Building	UNC	Off	Passive-on			LQR – CVL			H_2/LQG - CVL			OUV
				3V	6V	9V	3V	6V	9V	3V	6V	9V	
El centro, 1940	A	26.6	22.9	20.1	19.0	19.8	21.8	21.2	20.7	21.6	20.9	20.4	20.2
	B	17.1	8.1	8.6	10.4	11.5	8.4	8.6	8.7	8.6	9.1	9.6	8.8
Kobe, 1995	A	61.3	59.4	57.4	58.0	59.2	56.0	55.2	54.8	57.4	56.7	56.3	58.0
	B	48.0	35.0	25.6	30.6	32.9	29.6	27.5	26.0	30.5	27.7	25.5	30.7

Note: The displacement indicated is in × 10mm. UNC: incontrolled

Further, the results from **Error! Reference source not found.** show that there is not necessary to provide high command voltage for MR dampers and significant displacement response control is possible with less voltage in Building B. Using the optimum uniform voltage (OUV), the significant reduction for both buildings is observed under El-Centro 1940 earthquake although these proposed methods are not effectives in both buildings under Kobe 1995 earthquake. In **Error! Reference source not found.**, the top floor drift inter-storey responses show that the percentage reductions for Building A under passive-on strategy as compared to the uncontrolled case are: 8.0 under both the earthquakes. For Building B, the corresponding response reductions are 43.9 and 27.9 for El-Centro 1940 and Kobe 1995 earthquakes, respectively. However, marginal increase in response is seen under

semiactive controllers (9V) for Building B under El-Centro 1940 earthquake. **Error! Reference source not found.** shows that the percentage reductions in peak normalized base shear under passive-on strategy (6V) for both buildings are: 20 and 29.8 and under semiactive based on the reductions are 20 and 44 with El-Centro 1940.

Table 4: Peak top floor drift inter-storey under different control strategies

Earthquakes	Building	UNC	Off	Passive-on			LQR – CVL			H_2/LQG - CVL			OUV
				3V	6V	9V	3V	6V	9V	3V	6V	9V	
El centro, 1940	A	0.25	0.24	0.23	0.23	0.23	0.23	0.22	0.22	0.22	0.22	0.22	0.23
	B	0.41	0.26	0.23	0.28	0.31	0.29	0.37	0.43	0.33	0.41	0.51	0.32
Kobe, 1995	A	0.88	0.83	0.81	0.84	0.87	0.75	0.74	0.75	0.81	0.82	0.83	0.84
	B	1.54	1.19	1.11	0.98	1.07	0.84	0.99	1.21	0.84	0.88	1.02	1.35

Note: Peak top floor drift inter – story indicated is in × 10mm. UNC: Uncontrolled

Table 5: Peak normalized base shear under different control strategies

Earthquakes	Building	UNC	Off	Passive-on			LQR – CVL			H_2/LQG - CVL			OUV
				3V	6V	9V	3V	6V	9V	3V	6V	9V	
El centro, 1940	A	0.20	0.19	0.17	0.16	0.16	0.18	0.17	0.17	0.17	0.16	0.16	0.17
	B	0.57	0.28	0.35	0.40	0.40	0.29	0.30	0.31	0.29	0.32	0.35	0.35
Kobe, 1995	A	0.40	0.40	0.41	0.42	0.43	0.39	0.39	0.38	0.38	0.37	0.37	0.42
	B	1.56	1.10	0.71	0.90	1.00	0.88	0.80	0.76	0.94	0.83	0.74	0.88

8. CONCLUSIONS

For enhancing the seismic performance of two adjacent buildings, an optimal design method for nonlinear hysteretic dampers is proposed. The stochastic linearization method helps estimate the stochastic responses of adjacent buildings coupled with nonlinear dampers in an efficient manner. As a result, the optimal design process can avoid numerous nonlinear time-history analyses. The numerical example of 10- and 20-storey buildings coupled with MR dampers demonstrate that providing high command voltage is not necessary based on effectiveness of MR dampers. Moreover, the proposed optimal design approach can systematically achieve enhanced seismic performance with economical efficiency.

APPENDIX I- NOTATIONS

A = system matrix in state space equation

A_c = hysteresis loop parameters

a = constant value

a_j = each random number (j= 1, 2, .. popsize) between 0 and 1

a_{a0}, a_{b0} = proportional coefficients of Building A and Building B, respectively

B = system matrix in state space equation

b_{a0}, b_{b0} = proportional coefficients of Building A and Building B, respectively
C = damping matrix
C_p = constant value (1 or 2)
C_w = regulation matrix
C_1 = damping matrix of Building A
C_2 = damping matrix of Building B
c_d = damping of the damper
c_0 = hysteresis loop parameters of MR damper
c_{0a} = hysteresis loop parameters of MR damper
c_{0b} = hysteresis loop parameters of MR damper
c_1 = hysteresis loop parameters of MR damper
c_{1a} = hysteresis loop parameters of MR damper
c_{1b} = hysteresis loop parameters of MR damper
D = zero matrix in Hamiltonian
D_w = regulation matrix
d_i = inter-storey drift of the i^{th} floor in controlled system
d_{max} = the peak uncontrolled floor drift
E = system matrix in state space equation
E_1 = vector representing the influence of the related earthquake to Building A
E_2 = vector representing the influence of the related earthquake to Building B
F = fitness function
f_d = desired force matrix at the damper
f_{di} = desired force at the i^{th} damper
f_{mr} = force matrix at the damper
$\hat{G}_\infty$ = transfer function
$\left\|\hat{G}_\infty\right\|$ = H_∞ norm of $\hat{G}_\infty$
G^p = individual in the population
g_{rj}^{pi} = one variable in G^p
H_2 = control algorithm
H_∞ = control algorithm
$\boldsymbol{H}$ = Hamiltonian
$\mathbf{H}\{\ \}$ = Heaviside function in Matlab
h_j = bit string no. (j+1) starting from right

i_s = index

I = identity vector

$\mathbf{I}, \boldsymbol{I}$ = $(n+m)$ and $(2n+2m)$ identity matrices, respectively

J = objective function

$\mathbf{J}$ = performance index

J_1 = objective function to be minimized the displacement responses

J_2 = objective function to be minimized the inter-storey drift responses

j_s = index

K = stiffness matrix of all system

$\mathbf{K}$ = gain matrix

K_1 = stiffness matrix of Building A

K_2 = stiffness matrix of Building B

k_d = stiffness of the damper

k_0 = hysteresis loop parameters of MR damper

k_1 = hysteresis loop parameters of MR damper

L_i = lower bound value of design variable

l_m = length of sub-chromosome

M = total mass matrix

M_1 = mass matrix of Building A

M_2 = mass matrix of Building B

m = number of floors in Building B

m_i, m_j = mass $(i=1, 2, .., n)$ $(j=1, 2, .., m)$

m_a = number of measurements

N_d = total number of dampers at all floors

n = number of floors in Building A

n_a = number of actuators

$nbits$ = number of bits

n_d = hysteresis loop parameters of MR damper

n_r = random number

P = Riccati matrix, matrix of Lyapunov equation

P_i = significant digit

P_1 = control force location matrix of Building A

P_2 = control force location matrix of Building B

p_c = crossover rate

p_m = mutation rate
$\mathbf{Q}$ = state weighting matrix
q_j = probability of crossover
R =unit matrix having a random coefficient
R = scalar control force weighting matrix
$\mathbf{R}$ = control force weighting matrix
r_i = real number of a design variable
S = solution of the algebraic Ricatti equation
$S_{\ddot{x}_g\ddot{x}_g}, S_{v_i v_i}$ = spectral density function of acceleration and measurement noise
s = difference between the number floors of both buildings
s = Laplace variable
t = time
t_i = integer mapping of a binary string
U_i = upper bound value of design variable
$u, \dot{u}$ = control voltage and output of a first-order filter
V_{max} = maximum voltage
v = input voltages of the first order filter
v = measurement noise vector
$X, \dot{X}, \ddot{X}$ = total displacement, velocity and acceleration matrices, respectively
X_1, X_2 = displacement matrix of Building A and Building B, respectively
$\dot{X}_1, \dot{X}_2$ = velocity matrix of Building A and Building B, respectively
$\ddot{X}_1, \ddot{X}_2$ = acceleration matrix of Building A and Building B, respectively
$\ddot{X}_g$ = acceleration vector of the related earthquake
x^{max} = maximum displacement of the uncontrolled system
$x_i, \dot{x}_i$ = displacement and velocity of the i^{th} floor level, respectively
x_0 = initial displacement of the damper
y_m = vector of measured outputs
$y_i, \dot{y}_i$ = internal pseudo-displacement
$z_{di}, \dot{z}_{di}$ = evolutionary variable
$\alpha, \alpha_a, \alpha_b$ = hysteresis loop parameters of MR damper
α_c = weighting coefficient (1 or 2)
β = hysteresis loop parameters of MR damper
$\gamma, \gamma_u, \gamma_l$ =a random number, upper bound and lower bound of a positive number

ω_{ai}, ω_{aj}
ω_{bi}, ω_{bj} = structural modal frequencies of modes *i* and *j* of both buildings

ξ_{ai}, ξ_{aj}
ξ_{bi}, ξ_{bj} = structural damping ratios for modes *i* and *j* of both buildings

μ =constant to scale the fitness function

η = time constant of the first-order filter

Λ = system matrix in state space equation

Γ = vector representing the influence of the related earthquake to all system

0 = zero matrix

REFERENCES

1. Arfiadi Y, Hadi MNS. Optimum placement and properties of tuned mass dampers using hybrid genetic algorithms, *Int J Optim Civil Eng* 2011; **1**(1): 167-87.
2. Farshidianfar A, Soheili S. Optimized tuned liquid column dampers for earthquake oscillations of high-rise structures including soil effects, *Int J Optim Civil Eng* 2012; **2**(2): 221-34.
3. Farshidianfar A, Soheili S. Optimization of TMD parameters for earthquake vibrations of tall buildings including soil structure interaction, *Int J Optim Civil Eng* 2013; **3**(3): 409-29.
4. Ghasemi MR, Barghi E. Estimation of inverse dynamic behavior of MR dampers using artificial and fuzzy-based neural networks, *Int J Optim Civil Eng* 2012; **2**(3): 357-68.
5. Mohebbi M. Minimizing hankel's norm as design criterion of multiple tuned mass dampers**,** *Int J Optim Civil Eng* 2013; **3**(2): 271-88.
6. Mohebbi M, Bagherkhani A. Optimal design of magneto-rheological dampers, *Int J Optim Civil Eng* 2014; **4**(3): 361-80.
7. Mohebbi M, Moradpour S, Ghanbarpour Y. Improving the seismic behavior of nonlinear steel structures using optimal mtmds, *Int J Optim Civil Eng* 2014; **4**(1): 137-50.
8. Zhang WS, Xu YL. Dynamic characteristics and seismic response of adjacent buildings linked by discrete dampers, *Earthq Eng Struct Dyn* 1999; **28**(10) 1163-85.
9. Zhu HP, Ge DD, Huang X. Optimum connecting dampers to reduce the seismic responses of parallel structures, *J Sound Vib* 2011. **330**(9): p. 1931-1949.
10. Yang Z, Xu YL, Lu XL. Experimental seismic study of adjacent buildings with fluid dampers, *J Struct Eng* 2003; **129**(2): 197-205.
11. Zhang WS, Xu YL. Vibration analysis of two buildings linked by maxwell model-defined fluid dampers, *J Sound Vib* 2000; **233**(5): 775-96.
12. Bhaskararao AV, Jangid RS. Seismic analysis of structures connected with friction dampers, *Eng Struct* 2006; **28**(5): 690-703.
13. Hadi MNS, Uz ME. Investigating the optimal passive and active vibration controls of adjacent buildings based on performance indices using genetic algorithms, *J Eng Optim* 2015; **47**(2): 265-86.

14. Ng CL, Xu YL. Seismic response control of a building complex utilizing passive friction damper: experimental investigation, *Earthq Eng Struct Dyn* 2006; **35**(6): 657-77.
15. Bhaskararao AV, Jangid RS. Seismic response of adjacent buildings connected with friction dampers, *Bull Earthq Eng* 2006; **4**(1): 43-64.
16. Xu YL, Zhang WS. Closed-form solution for seismic response of adjacent buildings with linear quadratic Gaussian controllers, *Earthq Eng Struct Dyn* 2002; **31**(2): 235-59.
17. Ying ZG, Ni YQ, Ko JM. Stochastic optimal coupling-control of adjacent building structures, *Comput Struct* 2003; **81**(30-31): 2775-87.
18. Uz ME, Hadi M. Optimal design of semi active control for adjacent buildings connected by MR damper based on integrated fuzzy logic and multi-objective genetic algorithm, *J Eng Struct* 2014; **69**: 135-48.
19. Uz ME. Optimum design of semi-active dampers between adjacent buildings of different sizes subjected to seismic loading including soil-structure interaction, in *School of Civil, Mining Environ Eng* 2013, University of Wollongong, Wollongong.
20. Westermo B. The dynamics of interstructural connection to prevent pounding, *Earthq Eng Struct Dyn* 1989; **18**: 687-99.
21. Kim J, Ryu J, Chung L. Seismic performance of structures connected by viscoelastic dampers, *Eng Struct* 2006; **28**(2): 183-95.
22. Dyke SJ, et al. Acceleration feedback control of MDOF structures, *J Eng Mech* 1996; **122**(9): 907-18.
23. Ni YQ, Ko JM, Ying ZG. Random seismic response analysis of adjacent buildings coupled with non-linear hysteretic dampers, *J Sound Vib* 2001; **246**(3): 403-17.
24. Yoshida O, Dyke SJ. Seismic control of a nonlinear benchmark building using smart dampers, *J Eng Mech* 2004; **130**(4): 386-92.
25. Kaveh A, Sharafi P. Optimal priority functions for profile reduction using ant colony optimization, *Finite Elem Anal Des* 2008b; **44**(3): 131-8.
26. Sharafi P, Hadi M, Teh L. Heuristic Approach for Optimum Cost and Layout Design of 3D Reinforced Concrete Frames, *J Struct Eng* 2012; **138**(7): 853-63.
27. Sharafi P, Hadi M, Teh L. Geometric design optimization for dynamic response problems of continuous reinforced concrete beams, *J Comput Civil Eng* 2014; **28**(2): 202-9.
28. Sharafi P, Hadi MNS, Teh LH. Cost optimization of column layout design of reinforced concrete buildings, in *on the Maximization of the Fundamental Eigenvalue in Topology Optimization*, Gandomi A, Yang X, Talatahari S, Alavi A, Editors, Elsevier, London, 2013: pp. 129-146.
29. Sharafi P, Hadi MNS, Teh LH. Conceptual design optimization of rectilinear building frames-a knapsack problem approach, *Eng Optim* 2015; **47**(10): 331-41.
30. Sharafi P, Teh LH, Hadi MNS. Shape optimization of thin-walled steel sections using graph theory and ACO algorithm, *J Constr Steel Res* 2014; **101**: 331-41.
31. Luco JE, De Barros FCP. Optimal damping between two adjacent elastic structures, *Earthq Eng Struct Dyn* 1998; **27**(7): 649-59.
32. Ok SY, Song J, Park KS. Optimal design of hysteretic dampers connecting adjacent structures using multi-objective genetic algorithm and stochastic linearization method, *Eng Struct* 2008; **30**(5): 1240-9.

33. Bharti SD, Dumne SM, Shrimali MK. Seismic response analysis of adjacent buildings connected with MR dampers, *Eng Struct* 2010; **32**(8): 2122-33.
34. Ahlawat AS, Ramaswamy A. Multiobjective obtimal absorber system for torsionally coupled seismically excited structures, *Eng Struct* 2003; **25**: 941-50.
35. Arfiadi Y, Hadi MNS. Optimal direct (static) output feedback controller using real coded genetic algorithms, *Comput Struct* 2001; **79**(17): 1625-34.
36. Spencer JB, Dyke S, Sain M, Carlson J. Phenomenological model for magnetorheological dampers, *J Eng Mech* 1997; **123**(3): 230-8.
37. MATLAB. R2011b, The Math Works, Inc, Natick, MA.
38. Levine WS, Athans M. On the determination of the optimal constant output feedback gains for linear multivariable systems, *IEEE Trans Automat Contr* 1970; **15**(1): 44-8.
39. Lewis F, Syrmos V. Optimal Control. 1995, New York: John Wiley & Sons.
40. Motra GB, Mallik W, Chandiramani NK. Semi-active vibration control of connected buildings using magnetorheological dampers, *J Intell Mater Syst Struct* 2011; **22**(16): 1811-27.
41. Arfiadi Y. Optimal passive and active control mechanisms for seismically excited buildings, in *Faculty of Engineering*, University of Wollongong: Wollongong, 2000.
42. Abdel Raheem S, Hayashikawa T, Dorka U. Ground motion spatial variability effects on seismic response control of cable-stayed bridges, *Earthq Eng Struct Dyn* 2011; **10**(1): 37-49.
43. Yoshida O, Dyke SJ, Giacosa LM, Truman KZ. Experimental verification of torsional response control of asymmetric buildings using MR dampers, *Earthq Eng Struct Dyn* 2003; **32**(13): 2085-2105.
44. Spencer JBF, Suhardjo J, Sain MK. Frequency domain optimal control strategies for aseismic protection, *J Eng Mech* 1994; **120**(1): 135-58.
45. Pourzeynali S, Lavasani HH, Modarayi AH. Active control of high rise building structures using fuzzy logic and genetic algorithms, *Eng Struct* 2007; **29**(3): 346-57.